Research on parametric modeling and grinding methods of bottom edge of toroid-shaped end milling cutter

Lei Han[1], Xuefeng Cheng[1], Lei Jiang[1], Rong Li[1], Guofu Ding[1], Shengfeng Qin[2]

[1]Institute of Advanced Design and Manufacturing, School of Mechanical Engineering, Southwest Jiaotong University, Chengdu, China

[2]School of Design, Northumbria University, Newcastle upon Tyne, UK

Corresponding author:

Guofu Ding, Institute of Advanced Design and Manufacturing, School of Mechanical Engineering, Southwest Jiaotong University, Chengdu, 610031, China

Email: dingguofu@163.com

Abstract

For a toroid-shaped end milling cutter to have multi-structure features of tooth offset center and introversion of bottom edge, this paper proposes a generalized parametric modeling method of the bottom edge, including a straight edge segment and a circular arc edge segment. And based on the parametric model this paper also deduces the corresponding tool path for grinding of the bottom edge's rake and flank faces. The parametric modeling method is based on the geometric analytic equations while the grinding method is driven by the proposed parametric model and the parameters of rake and flank faces. The two methods can be applied to a bottom edge of a cutter with multi-structure features to guarantee G^1 continuity at the two joints for connecting a circular arc edge with a straight edge and a conical helix edge respectively. In order to verify the accuracy of proposed methods, experiments were carried out. The modeling and grinding experimental results verified the accuracy and utility of the methods.

Key words

Toroid-shaped end milling cutter; bottom edge; parametric modeling method; grinding method; integrated tool design and manufacturing

1 Introduction

Toroid-shaped end milling cutter (TEMC) is widely used in manufacturing of complicated parts with free-form surfaces[1]. The main parts of cutting edges participated in milling are a straight edge, a circular arc edge and a conical helix edge shown in Fig. 1. TEMC has the advantages of high adaptability and machining efficiency compared with ball-end milling cutter under constant scallop-height cutting[2]. And it has the ability to produce the periphery of parts meeting with the bottom floor with fillets[3]. Also, this type of cutter has higher material removal rate and lower flank wear rate because bottom edge is more solid[4][5] and thus, the machining quality is much more stable[6] compared with flat-end milling cutter.

Generally, the straight edge on TEMC having a tooth offset to the bottom center can improve its strength, and introversion to reduce friction between bottom edge and machined surface. As shown in Fig. 1, h is the tooth offset distance and η is the dish angle. Meanwhile TEMC has smooth cutting edges to ensure the cutting continuity during machining. However, the multi-structure features lead to difficulties in parametric modeling and grinding. Although there is a complete set of theory that can be used to design and manufacture TEMC without multi-structure features at present, it cannot be applied directly to TEMC with multi-structure features. Therefore the research on parametric modeling and grinding methods of this kind of TEMC is of great significance.

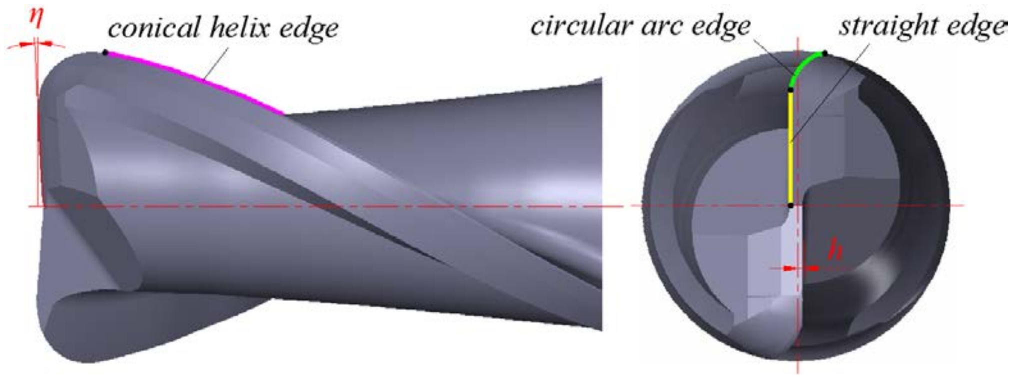

Fig. 1 Main parts of cutting edges (Straight edge has multi-structure features)

Precise parametric modeling of a bottom edge which determines the structure of end milling cutter is an essential for grinding of TEMC. Furthermore, the edge curve is also the guideline of the grinding wheel movement during grinding. Therefore parametric modeling of a bottom edge must be studied first. Many scholars have done much research about it. Chen adopted a supplementary cutting edge with a constant pitch to supply a general reference for TEMC with a constant angle between the cutting edge and the cutter axis[6]. Chen presented a precise mathematical modeling procedure for the design of cutters with a circular arc edge, the cutting edge forms a constant angle with the longitude curve[7], and presented a systematically design model of the involute end-milling cutter which cutting edge curves forms a constant angle with the cutter axis[8]. Chen presented a design model of TEMC, the cutting edge forms an approximately constant angle with the cutter axis[9]. Lin proposed a geometrical model of the cutting edge on TEMC with a constant angle between the cutting edge and the cutter axis[10]. Hsieh derived a mathematical model of the ideal conical helix edge which formed a constant angle to the longitudinal line at the toroid surface[11]. Tang studied the design models of the cutting edge with the convex curve generatrix, and put forward three mathematical models, i.e., planar cutting edges, helical cutting edges with a constant angle to the meridian and helical cutting edges with a constant pitch to avoid the problem of the inexistence of the cutting edge in the area near the end face of a cutter and the cutting edges are smoothly connected[12][13]. Yang introduced the design of a cutting edge with equal pitch, and the edge was continuous at the joint of the circular torus and the cylindrical surface[14]. Han gave the design method of the cutting edge which was defined as an approximate equal pitch curve with a concave arc as generator[15]. Lv established a mathematic model using infinitesimal geometry for the cutting edge design which used equal lead helix[16][17]. Although references [1], [18] and [19] used the generalized mathematical model proposed by Engin and Altintas[3][20][21], and seven geometric parameters were defined, if the circular torus is not a full quarter, there will be a discontinuity on the bottom edge. Cheng used the orthogonal helix edge curve as the S-shaped edge curve of ball-end milling cutter, the edge curve acquired based on the mathematical model proposed has a good S-shape and can connect with the circumferential edge curve smoothly. Furthermore, the model can be used easily to establish the S-shaped edge curve with tooth offset center or without tooth offset center[22].

Until now, several kinds of curves are used as a bottom edge on TEMC, such as an equal pitch edge curve, an equal helix angle edge curve with the longitude line, an equal helix angle edge curve with the cutter axis, a planar edge curve and an orthogonal helix edge curve. They have good edge curve shapes and can be used in series types of TEMC. However, present modeling methods using these kinds of curves are not concerned with a straight edge, not to mention the straight edge with multi-structure features, thus leading to complexity and difficulty of the grinding method. The grinding methods of TEMC are also studied by many scholars. Liu proposed a grinding process of the rake and flank faces and calculated the tool path and direction vector of grinding wheel[4]. Chen obtained the sectional profile of the grinding wheel by using an inverse problem-solving technique and the manufacturing model presented can be used on a two-axis NC machine[7]. Lin provided grinding models of a section design, feeding speeds and relative position of the grinding wheel[10]. Hsieh developed a systematic method for the grinding of the helical flute and the cutting edge, and considered the section profile and relative feeding velocities of the grinding wheel[11]. Bao studied a virtual two-axis grinding model of TEMC with an equal helix lead cutting edge and an equal helix angle cutting edge respectively[23].

In the above studies, many scholars focused on the parametric modeling and grinding methods of TEMC without multi-structure features of tooth offset to the center and introversion of the bottom edge. And thus the existing research results are just in a limited scope of application of the methods presented and no unified model is formed. In order to meet the requirements of the design and manufacturing of a toroid-shaped end milling cutter especially its bottom edge has multi-structure features, this article presents a generalized parametric modeling method of a bottom edge, and based on this, a grinding method for the rake and flank faces of the bottom edge can make the cutting edges with G^1 continuity, that is (1) the cutting edge curves meet at the joint points and (2) their tangent directions at the joints are the same. The G^1 continuity makes the composite cutting edge smooth. The modeling and grinding experiments indicates that the proposed cutter modelling and grinding methods can shorten the production cycle and improve the success rate of the design of a toroid-shaped end milling cutter, thus reduce the cost of cutter production. Furthermore, the proposed general and parametric modelling of a TEMC has a great potential to support optimal cutter design for different machining applications and the corresponding grinding method can easily realize the cutter design into tool manufacturing. This provides an integrated cutting design and manufacturing solution for wider applications.

This article is organized as follows: Section 2 describes the mathematical model of a bottom edge with multi-structure features of tooth offset center and introversion. Section 3 presents a grinding method of a bottom edge based on its 3D mathematical model. The experiments and results are described in section 4, and finally conclusions are drawn in section 5.

2 Parametric modeling method of bottom edge

Among many kinds of curves mentioned above, the planar edge curve has a good curve shape and more simple mathematical computation compared with others. This type of edge curve can reach G^1 continuity at the two joints of a circular arc edge with a straight edge and a conical helix edge respectively, and the straight edge can have multi-structure features whether or not. So planar edge curve is adopted, i.e., the circular arc edge is the intersecting planar curve of the circular torus and the plane composed of an extended line of straight edge and a tangential line at the end of the conical helix edge.

As shown in Fig. 2, the revolving surfaces of the cutting edges on TEMC are defined as three parts: a circular truncated conical surface *A* where the conical helix edge *a* lies, a circular torus *B* where the circular arc edge *b* lies, and a concave conical surface *C*. Their relationship is that *B* is tangent with *A* and *C*. Straight edge *c* has the multi-structure features of tooth offset center and introversion.

Define *I* as the intersection of *a* and *b*, *J* as the intersection of *b* and *c*. Define L_1 as the extended line of *c*, L_2 as the tangential line of *a* at *I*, L_3 as the intersecting line of *B* and *C*, L_4 as the intersecting line of *A* and *B*. Define *P* as the intersection of L_1 and L_2. Plane *M* is composed of L_1 and L_2. The bottom edge consists of *b* and *c*.

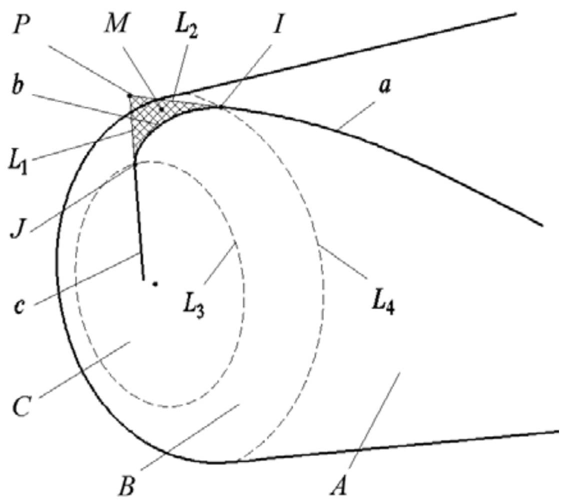

Fig. 2 Relevant geometrical elements of bottom edge

2.1 Parametric model of edge *c*

To reduce the complexity of mathematical modeling, define the coordinate system [O_1-$X_1Y_1Z_1$] as the first coordinate system, and the origin O_1 as center of *B*. Z_1 is the cutter axis and the positive direction is from the cutter shank to the tip. X_1 is parallel to the projection of *c* on the plane X_1Y_1. The point coordinates in the first coordinate system are identified by subscript _1.

Let γ be the angle between X_1-axis and the projection of IO_1 on the plane X_1Y_1. Rotate the first coordinate system on Z_1-axis by angle γ negatively, and the coordinate system [O_2-$X_2Y_2Z_2$] is obtained as the second coordinate system. The point coordinates in the second coordinate system are identified by subscript _2. Then, the parametric models of c and b can be described in the second coordinate system.

As shown in Fig. 3, define L as the intersection of L_3 and the plane X_1Z_1, Q as the tip of C, K as the endpoint of c, O_r as the center of the cross section of B on the plane X_1Z_1. Let r_e be the section radius of B, R be the distance between I and the cutter axis, κ be the half cone angle of A, β be the helix angle of a at I (angle between the helix edge on the revolving surface and the generator curve).

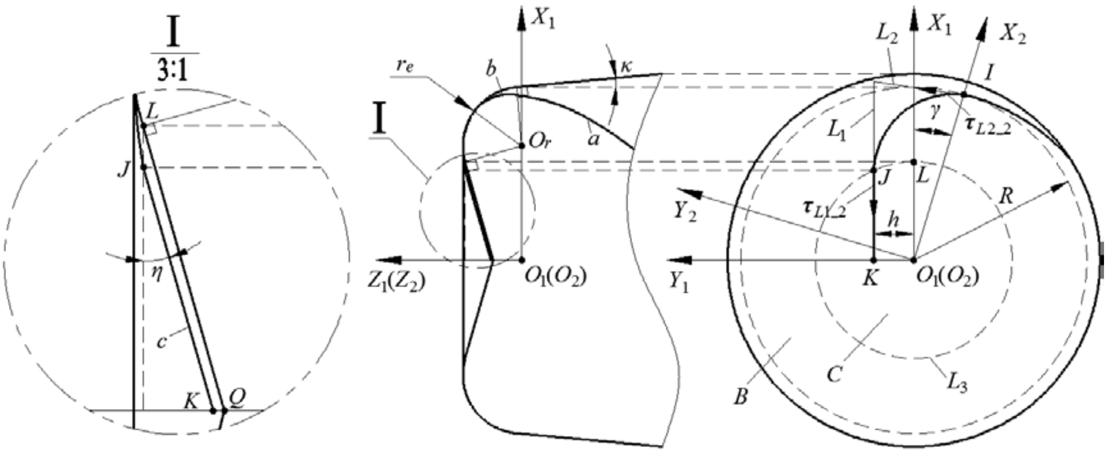

Fig. 3 Schematic diagram for the design of edge c

On the basis of cutter geometry relationship, the coordinates of J and K in the first coordinate system are as follows

$$\boldsymbol{J}_{\_1}=\begin{bmatrix} x_{J\_1} \\ y_{J\_1} \\ z_{J\_1} \end{bmatrix}=\begin{bmatrix} \sqrt{\left(x_{Or\_1}-r_e\cdot\sin\eta\right)^2-h^2} \\ h \\ r_e\cdot\cos\eta \end{bmatrix}, \tag{1}$$

$$\boldsymbol{K}_{\_1}=\begin{bmatrix} x_{K\_1} \\ y_{K\_1} \\ z_{K\_1} \end{bmatrix}=\begin{bmatrix} 0 \\ h \\ r_e\cdot\cos\eta-\sqrt{\left(x_{Or\_1}-r_e\cdot\sin\eta\right)^2-h^2}\tan\eta \end{bmatrix}. \tag{2}$$

According to the direction of the coordinate system, the rotation transformation matrix from the first coordinate system to the second coordinate system can be expressed as follows

$$\boldsymbol{T}_{1\_2}=\begin{bmatrix}\cos\gamma & \sin\gamma & 0\\ -\sin\gamma & \cos\gamma & 0\\ 0 & 0 & 1\end{bmatrix}. \tag{3}$$

Obviously, the coordinates of I can be described as

$$\boldsymbol{I}_{\_2}=\begin{bmatrix}x_{I\_2}\\ y_{I\_2}\\ z_{I\_2}\end{bmatrix}=\begin{bmatrix}R\\ 0\\ r_e\cdot\sin\kappa\end{bmatrix}, \tag{4}$$

where: $R=x_{Or\_1}+r_e\cdot\cos\kappa$.

Let $\boldsymbol{\tau}_{L1\_2}$, $\boldsymbol{\tau}_{L2\_2}$ be the unit direction vector of L_1 and L_2 respectively. Then $\boldsymbol{\tau}_{L1\_2}$ and the parametric equation $L_{1\_2}(t_1)$ of L_1 can be obtained by Eqs. (5) and (6) respectively

$$\boldsymbol{\tau}_{L1\_2}=\begin{bmatrix}\tau_{L1x\_2}\\ \tau_{L1y\_2}\\ \tau_{L1z\_2}\end{bmatrix}=\begin{bmatrix}-\cos\gamma\cdot\cos\eta\\ -\sin\gamma\cdot\cos\eta\\ -\sin\eta\end{bmatrix}, \tag{5}$$

$$L_{1\_2}(t_1)=\begin{cases}x=x_{J\_2}+t_1\cdot\tau_{L1x\_2},\\ y=y_{J\_2}+t_1\cdot\tau_{L1y\_2},\\ z=z_{J\_2}+t_1\cdot\tau_{L1z\_2}.\end{cases} \tag{6}$$

where t_1 is the independent variable.

Similarly, $\boldsymbol{\tau}_{L2\_2}$ and the parametric equation $L_{2\_2}(t_2)$ of L_2 can be obtained by Eqs. (7) and (8) respectively

$$\boldsymbol{\tau}_{L2\_2}=\begin{bmatrix}\tau_{L2x\_2}\\ \tau_{L2y\_2}\\ \tau_{L2z\_2}\end{bmatrix}=\begin{bmatrix}-\cos\beta\cdot\sin\kappa\\ \sin\beta\\ \cos\beta\cdot\cos\kappa\end{bmatrix}, \tag{7}$$

$$L_{2\_2}(t_2)=\begin{cases}x=x_{I\_2}+t_2\cdot\tau_{L2x\_2},\\ y=y_{I\_2}+t_2\cdot\tau_{L2y\_2},\\ z=z_{I\_2}+t_2\cdot\tau_{L2z\_2}.\end{cases} \tag{8}$$

where t_2 is the independent variable.

For L_1 and L_2 intersect at P, then

$$\begin{cases} x_{P\_2} = x_{J\_2} + t_1 \cdot \tau_{L1x\_2} = x_{I\_2} + t_2 \cdot \tau_{L2x\_2} \\ y_{P\_2} = y_{J\_2} + t_1 \cdot \tau_{L1y\_2} = y_{I\_2} + t_2 \cdot \tau_{L2y\_2} \\ z_{P\_2} = z_{J\_2} + t_1 \cdot \tau_{L1z\_2} = z_{I\_2} + t_2 \cdot \tau_{L2z\_2} \end{cases} . \tag{9}$$

So t_1, t_2 and γ can be obtained by Eqs. (5) to (9), shown as follows

$$\begin{cases} \sin\gamma = \dfrac{\left(y_{I\_2} + t_2 \cdot \tau_{L2y\_2}\right)\left(x_{J\_1} - t_1 \cdot \cos\eta\right) - \left(x_{I\_2} + t_2 \cdot \tau_{L2x\_2}\right) y_{J\_1}}{y_{J\_1}^2 + \left(x_{J\_1} - t_1 \cdot \cos\eta\right)^2}, \\ \cos\gamma = \dfrac{\left(x_{I\_2} + t_2 \cdot \tau_{L2x\_2}\right)\left(x_{J\_1} - t_1 \cdot \cos\eta\right) + \left(y_{I\_2} + t_2 \cdot \tau_{L2y\_2}\right) y_{J\_1}}{y_{J\_1}^2 + \left(x_{J\_1} - t_1 \cdot \cos\eta\right)^2}, \end{cases} \tag{10}$$

where: $t_1 = \dfrac{-T_2 + \sqrt{T_2^2 - 4T_1 \cdot T_3}}{2T_1}$;

$$t_2 = \frac{z_{J\_1} - z_{I\_2} - t_1 \cdot \sin\eta}{\tau_{L2z\_2}} ;$$

$$T_1 = \left(\tau_{L2x\_2}^2 + \tau_{L2y\_2}^2\right)\sin^2\eta - \tau_{L2z\_2}^2 \cdot \cos^2\eta ;$$

$$T_2 = 2\begin{Bmatrix} x_{J\_1} \cdot \tau_{L2z\_2}^2 \cdot \cos\eta - \left[\tau_{L2x\_2}\left(x_{I\_2} \cdot \tau_{L2z\_2} - z_{I\_2} \cdot \tau_{L2x\_2} + z_{J\_1} \cdot \tau_{L2x\_2}\right) + \right. \\ \left. \tau_{L2y\_2}\left(y_{I\_2} \cdot \tau_{L2z\_2} - z_{I\_2} \cdot \tau_{L2y\_2} + z_{J\_1} \cdot \tau_{L2y\_2}\right)\right]\sin\eta \end{Bmatrix} ;$$

$$\begin{aligned} T_3 = &\left(x_{I\_2} \cdot \tau_{L2z\_2} - z_{I\_2} \cdot \tau_{L2x\_2} + z_{J\_1} \cdot \tau_{L2x\_2}\right)^2 + \\ &\left(y_{I\_2} \cdot \tau_{L2z\_2} - z_{I\_2} \cdot \tau_{L2y\_2} + z_{J\_1} \cdot \tau_{L2y\_2}\right)^2 - \left(x_{J\_1}^2 + y_{J\_1}^2\right)\tau_{L2z\_2}^2 \end{aligned} .$$

For c and L_1 are collinear, the unit direction vector $\boldsymbol{\tau}_{c\_2}$ and parametric equation $c_{\_2}(t_1)$ of edge c can be obtained by Eqs. (5) and (6) respectively, and the range of t_1 is [0, $\left|x_{J\_2}/\tau_{L1x\_2}\right|$].

2.2 Parametric model of edge *b*

As shown in Fig. 4, define E as an arbitrary point on B, E' as the rotating projection of E on the plane X_1Z_1, N as an arbitrary point on bottom edge. Let θ be the angle between $E'O_r$ and X_1-axis (counter clockwise direction is positive), ϕ be the angle between the projection of EO_2 on the plane X_2Y_2 and X_2-axis (clockwise direction is positive).

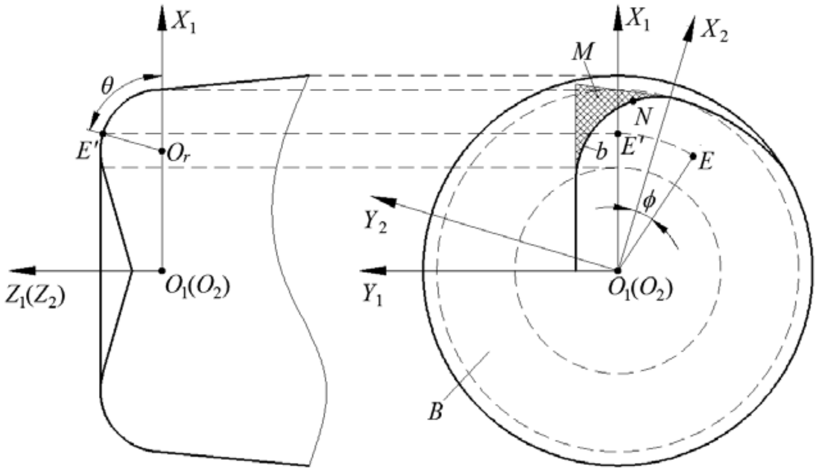

Fig. 4 Schematic diagram for the design of edge b

The normal vector $\boldsymbol{n}_{M\_2}$ of M is determined by the vector cross-product of $\boldsymbol{\tau}_{L1\_2}$ and $\boldsymbol{\tau}_{L2\_2}$ as follows

$$\boldsymbol{n}_{M\_2}=\begin{bmatrix} n_{Mx\_2} \\ n_{My\_2} \\ n_{Mz\_2} \end{bmatrix}=\boldsymbol{\tau}_{L1\_2}\times\boldsymbol{\tau}_{L2\_2}=\begin{bmatrix} \sin\beta\cdot\sin\eta-\cos\beta\cdot\cos\kappa\cdot\cos\eta\cdot\sin\gamma \\ \cos\beta\cdot\cos\kappa\cdot\cos\eta\cdot\cos\gamma+\cos\beta\cdot\sin\kappa\cdot\sin\eta \\ -\cos\beta\cdot\sin\kappa\cdot\cos\eta\cdot\sin\gamma-\sin\beta\cdot\cos\eta\cdot\cos\gamma \end{bmatrix}, \tag{11}$$

Hence, the equation of M can be obtained by Eq. (12)

$$n_{Mx\_2}\left(x-x_{I\_2}\right)+n_{My\_2}\left(y-y_{I\_2}\right)+n_{Mz\_2}\left(z-z_{I\_2}\right)=0. \tag{12}$$

By the definition of the circular torus[26], the parametric equation of B can be written as

$$B_{\_2}(\theta,\phi)=\begin{cases} x=\left(x_{Or\_1}+r_e\cdot\cos\theta\right)\cos\phi, \\ y=\left(x_{Or\_1}+r_e\cdot\cos\theta\right)\sin\phi, \quad \left(\kappa\le\theta\le\dfrac{\pi}{2}+\eta, 0\le\phi<2\pi\right). \\ z=r_e\cdot\sin\theta, \end{cases} \tag{13}$$

Since b is defined as a planar curve, then b is the intersecting line of M and B and angle ϕ can be determined by Eqs. (12) and (13)

$$\begin{cases} \sin\phi=\dfrac{n_{My\_2}\left(T_4-n_{Mz\_2}\cdot r_e\cdot\sin\theta\right)-n_{Mx\_2}\sqrt{\left(n_{Mx\_2}^2+n_{My\_2}^2\right)\left(x_{Or\_1}+r_e\cdot\cos\theta\right)^2-\left(T_4-n_{Mz\_2}\cdot r_e\cdot\sin\theta\right)^2}}{\left(n_{Mx\_2}^2+n_{My\_2}^2\right)\left(x_{Or\_1}+r_e\cdot\cos\theta\right)}, \\ \cos\phi=\dfrac{n_{Mx\_2}\left(T_4-n_{Mz\_2}\cdot r_e\cdot\sin\theta\right)+n_{My\_2}\sqrt{\left(n_{Mx\_2}^2+n_{My\_2}^2\right)\left(x_{Or\_1}+r_e\cdot\cos\theta\right)^2-\left(T_4-n_{Mz\_2}\cdot r_e\cdot\sin\theta\right)^2}}{\left(n_{Mx\_2}^2+n_{My\_2}^2\right)\left(x_{Or\_1}+r_e\cdot\cos\theta\right)}, \end{cases} \tag{14}$$

where: $T_4 = x_{I\_2} \cdot n_{Mx\_2} + y_{I\_2} \cdot n_{My\_2} + z_{I\_2} \cdot n_{Mz\_2}$.

Substituting Eq. (14) into Eq. (13) gives the parametric equation $b_{\_2}(\theta)$ of edge b

$$b_{\_2}(\theta) = \begin{cases} x = \dfrac{n_{Mx\_2}\left(T_4 - n_{Mz\_2} \cdot r_e \cdot \sin\theta\right) + n_{My\_2}\sqrt{\left(n_{Mx\_2}^2 + n_{My\_2}^2\right)\left(x_{Or\_1} + r_e \cdot \cos\theta\right)^2 - \left(T_4 - n_{Mz\_2} \cdot r_e \cdot \sin\theta\right)^2}}{\left(n_{Mx\_2}^2 + n_{My\_2}^2\right)}, \\ y = \dfrac{n_{My\_2}\left(T_4 - n_{Mz\_2} \cdot r_e \cdot \sin\theta\right) - n_{Mx\_2}\sqrt{\left(n_{Mx\_2}^2 + n_{My\_2}^2\right)\left(x_{Or\_1} + r_e \cdot \cos\theta\right)^2 - \left(T_4 - n_{Mz\_2} \cdot r_e \cdot \sin\theta\right)^2}}{\left(n_{Mx\_2}^2 + n_{My\_2}^2\right)}, \\ z = r_e \cdot \sin\theta, \end{cases} \quad \left(\kappa \le \theta \le \frac{\pi}{2} + \eta\right). \tag{15}$$

Take the derivative of Eq. (15) with respect to θ, the unit direction vector $\boldsymbol{\tau}_{b\_2}(\theta)$ of edge b can be expressed as

$$\boldsymbol{\tau}_{b\_2}(\theta) = \begin{bmatrix} \tau_{bx\_2} \\ \tau_{by\_2} \\ \tau_{bz\_2} \end{bmatrix} = \begin{bmatrix} \dfrac{-n_{My\_2} \cdot T_6 \cdot T_7 \cdot \sin\theta + n_{My\_2} \cdot n_{Mz\_2} \cdot T_5 \cdot \cos\theta - n_{Mx\_2} \cdot n_{Mz\_2}\sqrt{T_6 \cdot T_7^{\ 2} - T_5^{\ 2}}\cos\theta}{T_6\sqrt{T_6 \cdot T_7^{\ 2} - T_5^{\ 2} + \left(T_5 \cdot \sin\theta - T_7 \cdot n_{Mz\_2} \cdot \cos\theta\right)^2}} \\ \dfrac{n_{Mx\_2} \cdot T_6 \cdot T_7 \cdot \sin\theta - n_{Mx\_2} \cdot n_{Mz\_2} \cdot T_5 \cdot \cos\theta - n_{My\_2} \cdot n_{Mz\_2}\sqrt{T_6 \cdot T_7^{\ 2} - T_5^{\ 2}}\cos\theta}{T_6\sqrt{T_6 \cdot T_7^{\ 2} - T_5^{\ 2} + \left(T_5 \cdot \sin\theta - T_7 \cdot n_{Mz\_2} \cdot \cos\theta\right)^2}} \\ \dfrac{\sqrt{T_6 \cdot T_7^{\ 2} - T_5^{\ 2}}\cos\theta}{\sqrt{T_6 \cdot T_7^{\ 2} - T_5^{\ 2} + \left(T_5 \cdot \sin\theta - T_7 \cdot n_{Mz\_2} \cdot \cos\theta\right)^2}} \end{bmatrix}, \quad \left(\kappa \le \theta \le \frac{\pi}{2} + \eta\right), \tag{16}$$

where: $T_5 = T_4 - n_{Mz\_2} \cdot r_e \cdot \sin\theta$;

$T_6 = n_{Mx\_2}^2 + n_{My\_2}^2$;

$T_7 = x_{Or\_2} + r_e \cdot \cos\theta$.

2.3 The generalized helix angle of edge *b*

The parametric model of edge b is already obtained. Although edge b is a planar edge curve, it can be also regarded as a curve with a variable helix angle. At present, the generalized helix angle on the revolving surface has two definitions[24]: one is the angle between the helix edge on the revolving surface and the generator curve[22], the other is the angle between the helix edge on the revolving surface and the cutter axis[25]. The first definition is considered in this paper. The unit tangent vector of the generator curve of B at E can be expressed in the following form

$$\boldsymbol{\tau}_{BE\_2}(\theta)=\begin{bmatrix}-\sin\theta\cos\phi\\ \sin\theta\sin\phi\\ \cos\theta\end{bmatrix} \tag{17}$$

Hence the generalized helix angle at N can be given by

$$\begin{aligned}\beta_r&=\arccos\frac{\boldsymbol{\tau}_{BE\_2}(\theta)\cdot\boldsymbol{\tau}_{b\_2}(\theta)}{\left|\boldsymbol{\tau}_{BE\_2}(\theta)\right|\cdot\left|\boldsymbol{\tau}_{b\_2}(\theta)\right|}\\&=\arccos\frac{\sqrt{T_6\cdot T_7^{\,2}-T_5^{\,2}}}{\sqrt{T_6\cdot T_7^{\,2}-T_5^{\,2}+\left(T_5\cdot\sin\theta-T_7\cdot n_{Mz\_2}\cdot\cos\theta\right)^2}},\quad\left(\kappa\le\theta\le\frac{\pi}{2}+\eta\right).\end{aligned} \tag{18}$$

2.4 Parametric model of edge *a*

As shown in Fig. 5, define F as an arbitrary point on a. Let φ be the angle between the projection of FO_2 on the plane X_2Y_2 and X_2-axis (clockwise direction is positive).

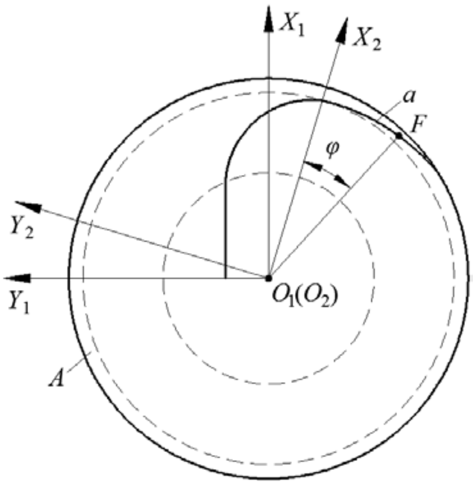

Fig. 5 Schematic diagram for the design of edge *a*

By the definition of the generalized helix, the parametric equation $a_{\_2}(\varphi)$ of edge a can be written as

$$a_{\_2}(\varphi)=\begin{cases} x=x_{I\_2}\cdot e^{-\varphi\cdot\sin(-\kappa)\cdot\cot\beta}\cdot\cos\varphi, \\ y=-x_{I\_2}\cdot e^{-\varphi\cdot\sin(-\kappa)\cdot\cot\beta}\cdot\sin\varphi, \\ z=-\dfrac{x_{I\_2}\left[1-e^{-\varphi\cdot\sin(-\kappa)\cdot\cot\beta}\right]}{\tan(-\kappa)}+r_e\cdot\sin\kappa, \end{cases} \quad (\varphi\geq 0). \tag{19}$$

Take the derivative of Eq. (19) with respect to φ, the unit direction vector $\boldsymbol{\tau}_{a\_2}(\varphi)$ of edge a can be expressed as

$$\boldsymbol{\tau}_{a\_2}(\varphi)=\begin{bmatrix}\tau_{ax\_2}\\ \tau_{ay\_2}\\ \tau_{az\_2}\end{bmatrix}=\begin{cases} x=\dfrac{T_8}{\sqrt{T_8^2+T_9^2+T_{10}^2}}, \\ y=\dfrac{T_9}{\sqrt{T_8^2+T_9^2+T_{10}^2}}, \\ z=\dfrac{T_{10}}{\sqrt{T_8^2+T_9^2+T_{10}^2}}, \end{cases} \quad (\varphi\geq 0). \tag{20}$$

where: $T_8=-\sin\kappa\cdot\cot\beta\cdot\cos\varphi+\sin\varphi$;

$T_9=\sin\kappa\cdot\cot\beta\cdot\sin\varphi+\cos\varphi$;

$T_{10}=\cos\kappa\cdot\cot\beta$.

3 Grinding method of bottom edge

Parametric model of the bottom edge is the base of the tool path of the grinding wheel. Bottom edge is the intersection curve of rake face and flank face, and its structural parameters are guaranteed by the grinding process of the two faces. For TEMC has a complex structure and lots of parameters and the purpose of the grinding method in this paper is to guarantee the precision of parameters related to bottom edge, the detailed method of the section profile formation was not presented here for simplification purpose. For convenience, the tool path calculation is deduced in the first coordinate system thus the origin of programming is O_1 and grinding wheel wear is not considered.

3.1 Parameters of the grinding wheel

The profile of V-shaped grinding wheel and Cup-shaped grinding wheel can both be defined by three parameters. Let R_g (the radius of the big-end of the grinding wheel), H_g (the thickness of the grinding wheel) and α_g (the taper angle of the grinding wheel) be three given geometric parameters of the grinding wheel profile, shown in Fig. 6.

Define the coordinate system $[O_g\text{-}X_gY_gZ_g]$ as the grinding wheel coordinate system, and the origin O_g as the center of the big-end of the grinding wheel, Z_g as the grinding wheel axis. Let $\boldsymbol{n}_{-1}$ (the unit direction vector of Z_g-axis) and $\boldsymbol{P}_{-1}$ (the coordinates of the origin O_g) be two parameters of tool path in the first coordinate system. Define v as the inclined angle in grinding process. Let v be v' in rake face grinding and let v be v'' in flank face grinding.

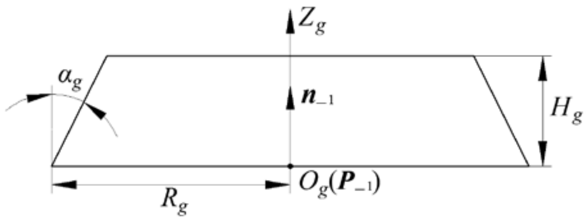

Fig. 6 Geometric parameters of the profile of grinding wheel

3.2 Grinding tool path for rake face

The grinding of the rake face of bottom edge is to form the chip-breaker-groove of the end cutting edge and the normal rake angle of TEMC.

Define the coordinate system $[O_n\text{-}X_nY_nZ_n]$ as the movable normal-section local coordinate system, the origin O_n coincides with N, Z_n-axis is tangent to the bottom edge and X_n-axis and the cutter axis lies in the same plane. In the grinding process, v' (the inclined angle restrained by the depth of chip-breaker-groove in rake face grinding) and γ_n (the normal rake angle of bottom edge) are pre-designed.

In a rake face grinding process, the coordinate system $[O'_g\text{-}X'_gY'_gZ'_g]$ can be obtained from the coordinate system [O_n-$X_nY_nZ_n$] by the following steps: rotate the coordinate system [O_n-$X_nY_nZ_n$] around Z_n-axis by angle γ_n positively, then around Y_n-axis by angle v' negatively, around X_n-axis by 90° negatively, at last translate the rotated coordinate system from O_n to O'_g to get the grinding wheel coordinate system.

Let $\boldsymbol{N}_{\_1}=[x_{N\_1}, y_{N\_1}, z_{N\_1}]^T$ be the coordinates of N in the first coordinate system. Define $\boldsymbol{T}_{1\text{-}n}$ and $\boldsymbol{R}_{1\text{-}n}$ as translation and rotation homogeneous transformation matrix(HTM) from the coordinate system [O_1-$X_1Y_1Z_1$] to [O_n-$X_nY_nZ_n$] respectively, $\boldsymbol{T}'_{n\text{-}g}$ and $\boldsymbol{R}'_{n\text{-}g}$ as translation and rotation HTM from the coordinate system [O_n-$X_nY_nZ_n$] to [O'_g-$X'_gY'_gZ'_g$] in rake face grinding process respectively as shown in Fig. 7. They can be obtained by Eqs. (19) to (22)

$$\boldsymbol{T}_{1-n}=\begin{bmatrix}1&0&0&x_{N\_1}\\0&1&0&y_{N\_1}\\0&0&1&z_{N\_1}\\0&0&0&1\end{bmatrix} \tag{21}$$

$$\boldsymbol{R}_{1-n}=\begin{bmatrix}\cos\theta&0&-\sin\theta&0\\0&1&0&0\\\sin\theta&0&\cos\theta&0\\0&0&0&1\end{bmatrix}\begin{bmatrix}1&0&0&0\\0&\cos\beta_r&\sin\beta_r&0\\0&-\sin\beta_r&\cos\beta_r&0\\0&0&0&1\end{bmatrix},\left(\kappa\le\theta\le\frac{\pi}{2}+\eta\right) \tag{22}$$

$$\boldsymbol{T}'_{n-g}=\begin{bmatrix}1&0&0&0\\0&1&0&R_g\\0&0&1&0\\0&0&0&1\end{bmatrix} \tag{23}$$

$$\boldsymbol{R}'_{n-g}=\begin{bmatrix}\cos\gamma_n&-\sin\gamma_n&0&0\\\sin\gamma_n&\cos\gamma_n&0&0\\0&0&1&0\\0&0&0&1\end{bmatrix}\begin{bmatrix}\cos v_1&0&-\sin v_1&0\\0&1&0&0\\\sin v_1&0&\cos v_1&0\\0&0&0&1\end{bmatrix}\begin{bmatrix}1&0&0&0\\0&0&1&0\\0&-1&0&0\\0&0&0&1\end{bmatrix} \tag{24}$$

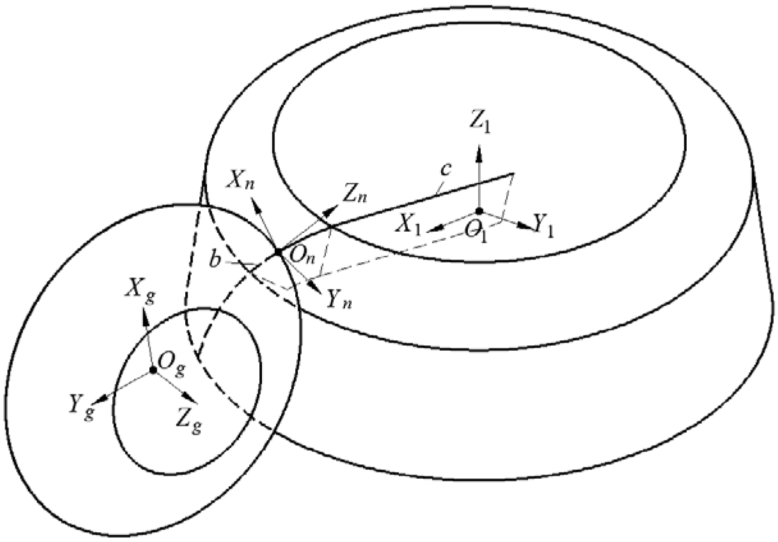

Fig. 7 Schematic diagram for rake face grinding

(1) The vector of the grinding wheel axis

According to the HTM theory, the vector of the grinding wheel axis in rake face grinding can be expressed as follows

$$\boldsymbol{n}'_{\_1} = \boldsymbol{R}_{1-n}\boldsymbol{R}'_{n-g}\begin{bmatrix}0 & 0 & 1 & 0\end{bmatrix}^T \tag{25}$$

(2) The position of CL point

According to the HTM theory, the position of CL point in rake face grinding can be expressed in the following form

$$\boldsymbol{P}'_{\_1} = \boldsymbol{T}_{1-n}\boldsymbol{R}_{1-n}\boldsymbol{R}'_{n-g}\boldsymbol{T}'_{n-g}\begin{bmatrix}0 & 0 & 0 & 1\end{bmatrix}^T \tag{26}$$

3.3 Grinding tool path for flank face

The grinding of the flank face of bottom edge is to form the normal relief angle of TEMC.

In the grinding process, v'' (the inclined angle to avoid interference between grinding wheel and other tooth in flank face grinding) and α_n (the normal relief angle of bottom edge) are pre-designed.

In a flank face grinding process, the coordinate system [O''_g-$X''_gY''_gZ''_g$] can be obtained from the coordinate system [O_n-$X_nY_nZ_n$] by the following steps: rotate the coordinate system [O_n-$X_nY_nZ_n$] around Z_n-axis by angle α_n negatively, then around

X_n-axis by angle v'' positively, around Y_n-axis by 90° negatively, at last translate the rotated coordinate system from O_n to O''_g to get the grinding wheel coordinate system for flank face grinding.

Define $\boldsymbol{T}''_{n\text{-}g}$ and $\boldsymbol{R}''_{n\text{-}g}$ as translation and rotation HTM from coordinate system $[O_n\text{-}X_nY_nZ_n]$ to $[O''_g\text{-}X''_gY''_gZ''_g]$ in flank face grinding process respectively as shown in Fig. 8. They can be obtained by Eqs. (25) and (26)

$$\boldsymbol{T}''_{n-g} = \begin{bmatrix} 1 & 0 & 0 & R_{g2} \\ 0 & 1 & 0 & 0 \\ 0 & 0 & 1 & 0 \\ 0 & 0 & 0 & 1 \end{bmatrix} \tag{27}$$

$$\boldsymbol{R}''_{n-g} = \begin{bmatrix} \cos\alpha_n & \sin\alpha_n & 0 & 0 \\ -\sin\alpha_n & \cos\alpha_n & 0 & 0 \\ 0 & 0 & 1 & 0 \\ 0 & 0 & 0 & 1 \end{bmatrix} \begin{bmatrix} 1 & 0 & 0 & 0 \\ 0 & \cos\nu_2 & -\sin\nu_2 & 0 \\ 0 & \sin\nu_2 & \cos\nu_2 & 0 \\ 0 & 0 & 0 & 1 \end{bmatrix} \begin{bmatrix} 0 & 0 & 1 & 0 \\ 0 & 1 & 0 & 0 \\ -1 & 0 & 0 & 0 \\ 0 & 0 & 0 & 1 \end{bmatrix} \tag{28}$$

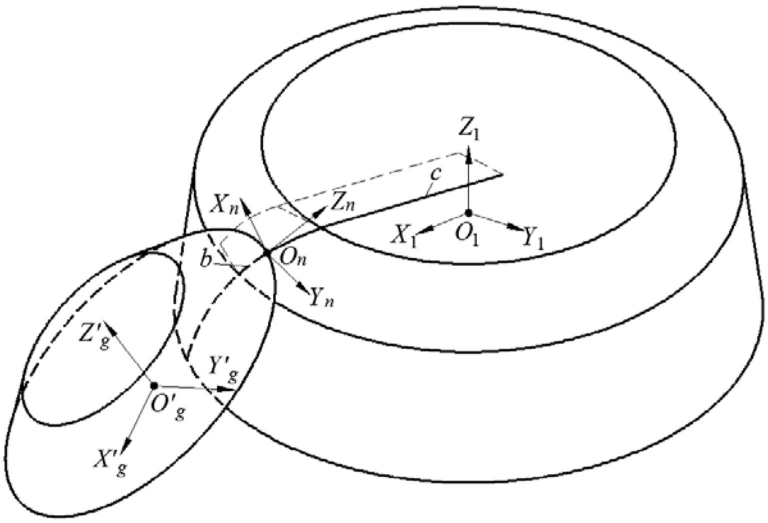

Fig. 8 Schematic diagram for flank face grinding

(1) The vector of the grinding wheel axis

According to the HTM theory, the vector of the grinding wheel axis in flank face grinding can be expressed as follows

$$\boldsymbol{n}''_{\_1} = \boldsymbol{R}_{1-n}\boldsymbol{R}''_{n-g}\begin{bmatrix} 0 & 0 & 1 & 0 \end{bmatrix}^T \tag{29}$$

(2) The position of CL point

According to the HTM theory, the position of CL point in flank face grinding can be expressed in the following form

$$\boldsymbol{P}''_{\_1} = \boldsymbol{T}_{1-n}\boldsymbol{R}_{1-n}\boldsymbol{R}''_{n-g}\boldsymbol{T}''_{n-g}\begin{bmatrix}0 & 0 & 0 & 1\end{bmatrix}^T \tag{30}$$

4 Experiments and results

4.1 Modeling experiment

To verify the validity of the proposed parametric modeling method, modeling experiment was carried out in MATLAB. To validate the G^1 continuity at the two joints of a circular arc edge with the connected straight edge and conical helix edge, one TEMC with multi-structure features of tooth offset center and introversion of its straight edge was taken for example. The design values related to parametric modeling of the cutting edge are shown in Table 1.

Table 1 Design values related to parametric modeling of the cutting edge

Parameters	$2R$ (mm)	r_e (mm)	h (mm)	η (°)	κ (°)	β (°)
Design values	20	1.5	0.2	4	4.5	39

The calculated coordinates of J on c by substituting t_1=0 into Eq. (6) is set as $\boldsymbol{J}_{\_2c}$. The calculated coordinates of J on b by substituting $\theta=\pi/2+\eta$ into Eq. (15) is set as $\boldsymbol{J}_{\_2b}$. The calculated coordinates of I on b by substituting $\theta=\kappa$ into Eq. (15) is set as $\boldsymbol{I}_{\_2b}$. The calculated coordinates of I on a by substituting φ=0 into Eq. (19) is set as $\boldsymbol{I}_{\_2a}$. The calculated unit tangential vector of c at J by Eq. (5) is set as $\boldsymbol{\tau}_{J\_2c}$. The calculated unit tangential vector of b at J by substituting $\theta=\pi/2+\eta$ into Eq. (16) is set as $\boldsymbol{\tau}_{J\_2b}$. The calculated unit tangential vector of b at I by substituting $\theta=\kappa$ into Eq. (16) is set as $\boldsymbol{\tau}_{I\_2b}$. The calculated unit tangential vector of a at I by substituting φ=0 into Eq. (20) is set as $\boldsymbol{\tau}_{I\_2a}$. The modeling parameters of one tooth are shown in Table 2 and the result in MATLAB is shown in Fig. 9.

Table 2 Modeling parameters

Equations	Conditions	Parameters	Calculated values
Eq. (6)	t_1=0	$\boldsymbol{J}_{\_2c}$ (mm)	$[8.3341, 1.0504, 1.4963]^T$
Eq. (15)	$\theta=\pi/2+\eta$	$\boldsymbol{J}_{\_2b}$ (mm)	$[8.3341, 1.0504, 1.4963]^T$
Eq. (15)	$\theta=\kappa$	$\boldsymbol{I}_{\_2b}$ (mm)	$[10.0000, 0.0000, 0.1177]^T$
Eq. (19)	φ=0	$\boldsymbol{I}_{\_2a}$ (mm)	$[10.0000, 0.0000, 0.1177]^T$
Eq. (5)	\	$\boldsymbol{\tau}_{J\_2c}$	$[-0.9924, -0.1014, -0.0698]^T$
Eq. (16)	$\theta=\pi/2+\eta$	$\boldsymbol{\tau}_{J\_2b}$	$[-0.9924, -0.1014, -0.0697]^T$
Eq. (16)	$\theta=\kappa$	$\boldsymbol{\tau}_{I\_2b}$	$[-0.0610, 0.6293, 0.7748]^T$
Eq. (20)	φ=0	$\boldsymbol{\tau}_{I\_2a}$	$[-0.0610, 0.6293, 0.7748]^T$

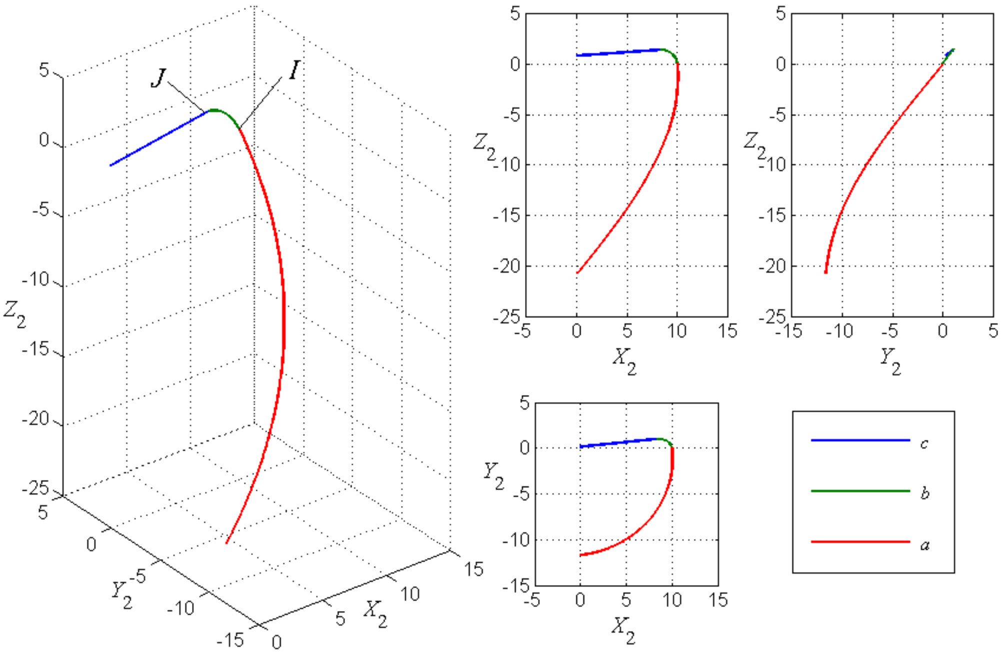

Fig. 9 Modeling result of the bottom edge and the conical helix edge in MATLAB

The calculated and modeling results validate the G^1 continuity at the two joints and prove the accuracy of the parametric modeling method.

4.2 Grinding experiment

The machining accuracy of the grinding tool path was verified by the grinding experiment. The parameters of the grinding wheel profile and grinding process are shown in Table 3. The allowable absolute errors of machining are 0.1mm/0.5°.

Table 3 Parameters of the grinding wheel profile and grinding process

Grinding process	Parameters of grinding wheel					
	Shape	Type	R_g (mm)	H_g (mm)	α_g (°)	ν(°)
Rake face grinding	V-shape	12V9	50	25	45	75
Flank face grinding	Cup-shape	11V9	50	32	30	60

Based on the mathematical models of TEMC, the grinding tool path in grinding of the tested TEMC was calculated by the grinding method put forward. Part of the grinding tool path file obtained by the grinding method put forward is shown below

"......

GOTO/34.687784, -1.083085, -3.482481, -0.089849, 0.769583, -0.632194

GOTO/34.688929, -1.095449, -3.472860, -0.089220, 0.769622, -0.632236

GOTO/34.690062, -1.107808, -3.463239, -0.088592, 0.769661, -0.632276

GOTO/34.691183, -1.120164, -3.453619, -0.087964, 0.769700, -0.632316

GOTO/34.692292, -1.132515, -3.444000, -0.087335, 0.769740, -0.632355

GOTO/34.693389, -1.144862, -3.434381, -0.086707, 0.769780, -0.632393

GOTO/34.694474, -1.157205, -3.424763, -0.086079, 0.769820, -0.632430

GOTO/34.695548, -1.169544, -3.415145, -0.085450, 0.769860, -0.632466

GOTO/34.696610, -1.181879, -3.405528, -0.084822, 0.769901, -0.632502

GOTO/34.697659, -1.194210, -3.395911, -0.084194, 0.769941, -0.632536

GOTO/34.698697, -1.206536, -3.386296, -0.083566, 0.769982, -0.632570

......"

The NC codes were generated by post-process from the grinding tool path and were verified in a grinding process. The material of TEMC was cemented carbide. The trial product grinded by ANCA FastGrind CNC cutter grinding machine tool is shown in Fig. 10.

Fig. 10 Trial product of TEMC

(1) Measurement of the major parameters

The major parameters of the trial product were measured by Zoller genius-3 tool measuring instrument using the principle of non-contact light perception scanning in no vibration environment and at room temperature. In the “ELEPHANT” module of the instrument, choose the parameters which require measurement and then the instrument can automatically measure the parameters within the accuracy of 0.001mm/0.01°. Measured the values three times over all different parameters and took the average as the final measured values to reduce measurement errors. The major design values and the corresponding trial product measured values are shown in Table 4.

Table 4 Comparison of major design and measured values

Parameters	$2R$ (mm)	r_e (mm)	h (mm)	η (°)	γ_n (°)	α_n (°)
Major design values	20	1.5	0.2	4	8	14
Trial product measured values	19.991	1.483	0.215	4.23	8.31	13.73

(2) Measurement of the bottom edge

The point cloud of the trial product was measured and obtained by Solutionix Rexcan Ⅲ 3D optical scanner within the accuracy of 0.007mm. The 3D optical scanning and the point cloud of the trial product are shown in Fig. 11.

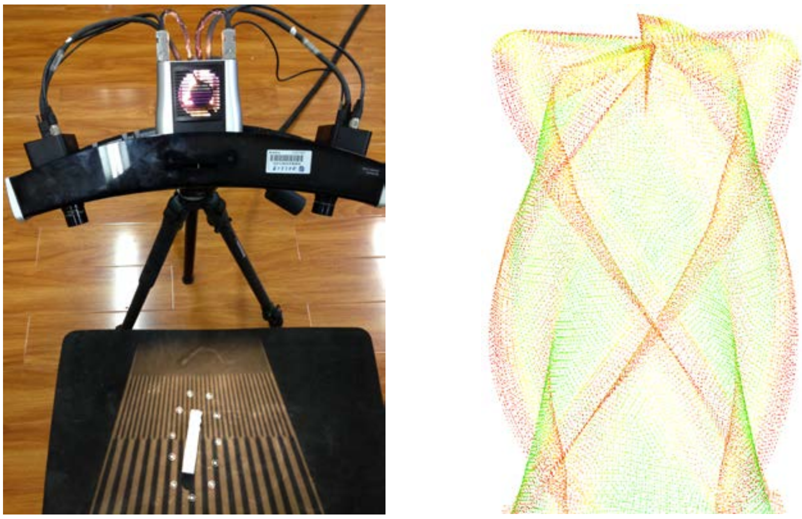

(a) 3D optical scanning (b) Point cloud

Fig. 11 3D optical scanning and point cloud of the trial product

In total, 31 points on edge *c* and 12 points on edge *b* were extracted from the point cloud (see Fig.11). The extracted points and the theoretical bottom edge are built up in MATLAB as shown in Fig. 12.

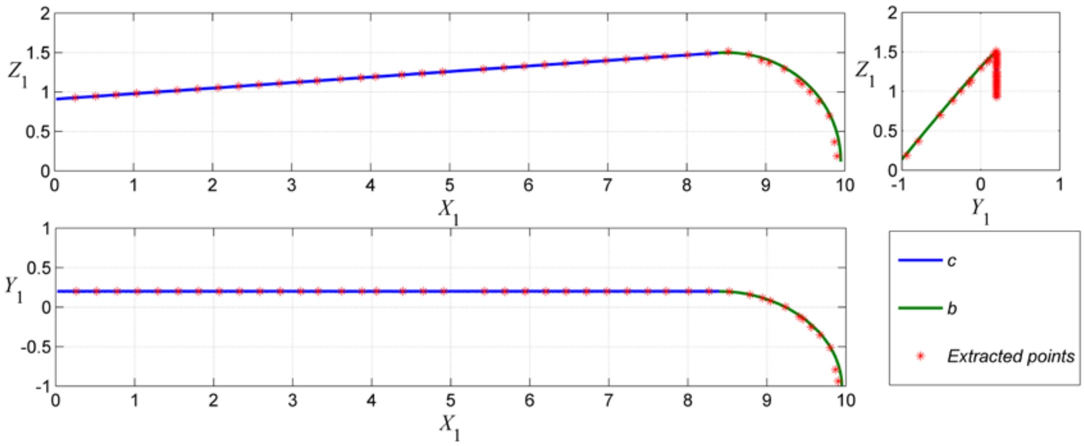

Fig. 12 The theoretical bottom edge and the extracted points

The coordinates of the extracted points were obtained and the distances between the extracted points and the theoretical bottom edge were calculated. The maximum distances for edge *c* and *b* are 0.021mm and 0.055mm separately.

According to the measurement results of the major parameters on the bottom edge, the maximum absolute errors of the trial product grinded by the proposed grinding method are 0.055mm/0.31°. And they are both within the allowable tolerance range. The precision of the major parameters and the edge position meets the requirement of machining, and the effectiveness of the tool path for grinding of the rake and flank faces of bottom edge is illustrated.

5 Conclusions

In this study, a generalized and accurate parametric modeling method and the corresponding grinding methods of a bottom edge of TEMC are presented. The bottom edge acquired based on this parametric modeling method can possess multi-structure features of tooth offset center or introversion. Furthermore, the parametric equations of the bottom edge are put forward, and the bottom edge can meet G^1 continuity at the two joints of a circular arc edge with a straight edge and a conical helix edge, respectively. The grinding method is driven by the parametric model of the bottom edge and the design values of its rake and flank faces. And it can realize the accurate calculation of the tool path for grinding. Finally, the utility and accuracy of the parametric modeling and grinding methods are verified through a serious of experiments.

It is believed that the proposed general and parametric modelling of the cutting edges of a TEMC with multi-features can be used to optimize cutter design for different application scenarios by setting up a proper set of parameters. Upon achieving the optimal cutter design, its corresponding grinding method is also ready to be applied effectively in the cutter (tool) manufacturing. Therefore, the integration of the cutter design modelling and the associated grinding method provide an integral solution for optimal cutter design and manufacturing.

Acknowledgement

This work is supported by the Special Fund of High-end CNC Machine Tools and Basic Manufacturing Equipment (2015ZX04001002), China.

References

[1] Gao G, Wu B, Zhang D, et al. Mechanistic identification of cutting force coefficients in bull-nose milling process[J]. Chinese Journal of Aeronautics, 2013, 26(3): 823-830.

[2] Chen T, Liu X, Wang C, et al. Design and fabrication of double-circular-arc torus milling cutter[J]. The International Journal of Advanced Manufacturing Technology, 2015: 1-13.

[3] Engin S, Altintas Y. Mechanics and dynamics of general milling cutters. Part I: helical end mills[J]. International Journal of Machine Tools and Manufacture, 2001, 41(15): 2195-2212.

[4] Liu J J, Li R, Cheng X F, et al. Research on CNC grinding simulation technology of torus end milling cutter’s end edges[J]. Modern Manufacturing Engineering, 2012, (10):84-89.

[5] Endres W J, Kountanya R K. The effects of corner radius and edge radius on tool flank wear[J]. Journal of Manufacturing Processes, 2002, 4(2): 89-96.

[6] Chen C B. Discussion on the problems related to NC machining of toroid-shaped taper cutter with constant angle between cutting edge and the cutter axis[J]. The International Journal of Advanced Manufacturing Technology, 2007, 35:493-504.

[7] Chen W F, Lai H Y, Chen C K. A Precision Tool Model for Concave Cone-End Milling Cutters[J]. The International Journal of Advanced Manufacturing Technology, 2001, 18(8): 567-578.

[8] Chen W F. A precision design for computer numerical control machining models of involute-generator revolving cutters[J]. Proceedings of the Institution of Mechanical Engineers, Part B: Journal of Engineering Manufacture, 2004, 218(5): 517-531.

[9] Chen W Y, Wang J C, Chen W F. A precision design and NC machining of circular-arc end-milling cutters[J]. Journal of Materials Processing and Manufacturing Science, 2001, 10: 45-67.

[10] Lin S W. Study on the 2-Axis NC Machining of a Toroid-Shaped Cutter with a Constant Angle Between the Cutting Edge and the Cutter Axis[J]. Journal of Materials Processing Technology, 2001, 115(3):338-343.

[11] Hsieh J M, Tsai Y C. Geometric modeling and grinder design for toroid-cone shaped cutters[J]. The International Journal of Advanced Manufacturing Technology, 2006, 29:912-921.

[12] Tang Y Y, Yao Q. Study on the toroidal convex milling cutter[J]. Journal of Harbin Institute of Technology, 2000, 17(1):22-24.

[13] Tang Y Y, Ren B Y. Two problems concerning 2-axis NC machining using toroid- shaped revolving cutter and their solutions[J]. Journal of Harbin Institute of Technology, 2002, 34(2):191-193.

[14] Yang X, Tang Y Y, Li W. On the toroidal columned milling cutter with equal screw pitch[J]. Journal of Jiamusi University (Natural Science Edition), 2000, 18(1):38-41.

[15] Han C S, Tang Y Y, Hou X Y. Research on non-numerical controlled machining concave arc revolving milling cutter[J]. Journal of Natural Science of Heilongjiang University, 2001, 18(4):29-32.

[16] Lv G M, Xue Y, Tang Y Y. The curve of constant pitch cutting of conical milling cutter with an angular circle[J]. Journal of Harbin Institute of Technology, 2004, 21(2):44-46.

[17] Lv G M, Wang H B, Tang Y Y, et al. Cutting edge curve models for equal pitch cutters and

their applications[J]. Journal of Harbin Institute of Technology, 2004, 11(1):46-48.

[18] Gradišek J, Kalveram M, Weinert K. Mechanistic identification of specific force coefficients for a general end mill[J]. International Journal of Machine Tools and Manufacture, 2004, 44(4): 401-414.

[19] Wan M, Zhang W H, Qin G H, et al. Efficient calibration of instantaneous cutting force coefficients and runout parameters for general end mills[J]. International Journal of Machine Tools and Manufacture, 2007, 47(11): 1767-1776.

[20] Engin S, Altintas Y. Generalized modeling of milling mechanics and dynamics: Part I–Helical end Mills[J]. Am. Soc. Mech. Eng. Manuf. Eng. Div.(MED), 1999, 10: 345-352.

[21] Altintas Y, Engin S. Generalized modeling of mechanics and dynamics of milling cutters[J]. CIRP Annals-Manufacturing Technology, 2001, 50(1): 25-30.

[22] Cheng X F, Ding G F, Li R, et al. A new design and grinding algorithm for ball-end milling cutter with tooth offset center[J]. Proceedings of the Institution of Mechanical Engineers, Part B: Journal of Engineering Manufacture, 2014, 228(7): 687-697.

[23] Bao Q S, Wang Y T, Tang Y Y, et al. A study on a virtual manufacturing model of a revolving milling cutter in 2-axis numerical control processing. Journal of Materials Processing Technology, 2002, 120(1): 68–75.

[24] Lai H Y, Chen W F. Precision design and numerical control machining of tapered ball-end milling cutters[J]. Proceedings of the Institution of Mechanical Engineers, Part B: Journal of Engineering Manufacture, 2002, 216(2): 183-197.

[25] Chen W F. A mathematical solution to the design and manufacturing problems of ball-end cutters having a cutting edge with constant angle to the axis[J]. Proceedings of the Institution of Mechanical Engineers, Part C: Journal of Mechanical Engineering Science, 2004, 218(3): 301-308.

[26] Department of Applied Mathematics, Tongji University. Advanced Mathematics[M]. Peking: Higher Education Press, 2002.7:320-322.

Appendix

Notation

a	conical helix edge
$a_{\_2}(\varphi)$	parametric equation of edge a in the second coordinate system
A	circular truncated conical surface
b	circular arc edge
$b_{\_2}(\theta)$	parametric equation of edge b in the second coordinate system
B	circular torus
$B_{\_2}(\theta, \phi)$	parametric equation of B in the second coordinate system
c	Straight edge
$c_{\_2}(t_1)$	parametric equation of edge c in the second coordinate system

C	concave conical surface
E	an arbitrary point on B
E'	rotating projection of E on the plane X_1Z_1
h	distance of tooth offset the center
H_g	thickness of the grinding wheel
I	intersection of a and b
$\boldsymbol{I}_{\_2}$	coordinates of I in the second coordinate system
$\boldsymbol{I}_{\_2a}$	calculated coordinates of I on a by substituting φ=0 into Eq. (19)
$\boldsymbol{I}_{\_2b}$	calculated coordinates of I on b by substituting $\theta=\kappa$ into Eq. (15)
J	intersection of b and c
$\boldsymbol{J}_{\_1}$	coordinates of J in the first coordinate system
$\boldsymbol{J}_{\_2}$	coordinates of J in the second coordinate system
$\boldsymbol{J}_{\_2b}$	calculated coordinates of J on b by substituting $\theta=\pi/2+\eta$ into Eq. (15)
$\boldsymbol{J}_{\_2c}$	calculated coordinates of J on c by substituting t_1=0 into Eq. (6)
K	endpoint of c
$\boldsymbol{K}_{\_1}$	coordinates of K in the first coordinate system
L	intersection of L_3 and the plane X_1Z_1
L_1	extended line of c
$L_{1\_2}(t_1)$	parametric equation of L_1 in the second coordinate system
L_2	tangential line of a at I
$L_{2\_2}(t_2)$	parametric equation of L_2 in the second coordinate system
L_3	intersecting line of B and C
L_4	intersecting line of A and B
M	plane composed of L_1 and L_2
N	arbitrary point on bottom edge
$\boldsymbol{n}_{\_1}$	unit direction vector of axis Z_g in the first coordinate system
$\boldsymbol{n}'_{\_1}$	vector of the grinding wheel axis in rake face grinding in the first coordinate system
$\boldsymbol{n}''_{\_1}$	vector of the grinding wheel axis in flank face grinding in the first coordinate

	system
$\boldsymbol{n}_{M\_2}$	normal vector of M in the second coordinate system
N	an arbitrary point on bottom edge
$\boldsymbol{N}_{\_1}$	coordinates of N in the first coordinate system
O_g	center of the big-end of the grinding wheel
O_r	center of the cross section of B on the plane X_1Z_1
$[O_1\text{-}X_1Y_1Z_1]$	first coordinate system
$[O_2\text{-}X_2Y_2Z_2]$	second coordinate system
$[O_g\text{-}X_gY_gZ_g]$	grinding wheel coordinate system
$[O'_g\text{-}X'_gY'_gZ'_g]$	grinding wheel coordinate system in rake face grinding
$[O''_g\text{-}X''_gY''_gZ''_g]$	grinding wheel coordinate system in flank face grinding
$[O_n\text{-}X_nY_nZ_n]$	normal-section local coordinate system
P	intersection of L_1 and L_2
$\boldsymbol{P}_{\_1}$	coordinates of the origin O_g in the first coordinate system
$\boldsymbol{P}'_{\_1}$	position of CL point in rake face grinding in the first coordinate system
$\boldsymbol{P}''_{\_1}$	position of CL point in flank face grinding in the first coordinate system
Q	tip of C
r_e	section radius of B
R	distance between I and the cutter axis
$\boldsymbol{R}_{1\text{-}n}$	rotation HTM from coordinate system $[O_1\text{-}X_1Y_1Z_1]$ to $[O_n\text{-}X_nY_nZ_n]$
R_g	radius of the big-end of the grinding wheel
$\boldsymbol{R}'_{n\text{-}g}$	rotation HTM from coordinate system $[O_n\text{-}X_nY_nZ_n]$ to $[O'_g\text{-}X'_gY'_gZ'_g]$
$\boldsymbol{R}''_{n\text{-}g}$	rotation HTM from coordinate system $[O_n\text{-}X_nY_nZ_n]$ to $[O''_g\text{-}X''_gY''_gZ''_g]$
$\boldsymbol{T}_{1\text{-}2}$	translation HTM from the first coordinate system to the second coordinate system
$\boldsymbol{T}_{1\text{-}n}$	translation HTM from coordinate system $[O_1\text{-}X_1Y_1Z_1]$ to $[O_n\text{-}X_nY_nZ_n]$
$\boldsymbol{T}'_{n\text{-}g}$	translation HTM from coordinate system $[O_n\text{-}X_nY_nZ_n]$ to $[O'_g\text{-}X'_gY'_gZ'_g]$
$\boldsymbol{T}''_{n\text{-}g}$	translation HTM from coordinate system $[O_n\text{-}X_nY_nZ_n]$ to $[O''_g\text{-}X''_gY''_gZ''_g]$
α_g	taper angle of the grinding wheel

α_n	normal relief angle of bottom edge
β	helix angle of a at I
β_r	generalized helix angle at N
γ	angle between the positive direction of X_1 and X_2
γ_n	normal rake angle of bottom edge
η	dish angle
θ	angle between $E'O_r$ and X_1-axis
κ	half cone angle of A
ν	the inclined angle in grinding process
ν'	the inclined angle in rake face grinding
ν''	the inclined angle in flank face grinding
$\boldsymbol{\tau}_{a\_2}(\varphi)$	unit direction vector of edge a in the second coordinate system
$\boldsymbol{\tau}_{b\_2}(\theta)$	unit direction vector of edge b in the second coordinate system
$\boldsymbol{\tau}_{BE\_2}(\theta)$	unit tangent vector of the generator curve of B at E in the second coordinate system
$\boldsymbol{\tau}_{c\_2}$	unit direction vector of edge c in the second coordinate system
$\boldsymbol{\tau}_{I\_2a}$	calculated unit tangential vector of a at I by substituting φ=0 into Eq. (20)
$\boldsymbol{\tau}_{I\_2b}$	calculated unit tangential vector of b at I by substituting θ=κ into Eq. (16)
$\boldsymbol{\tau}_{J\_2b}$	calculated unit tangential vector of b at J by substituting θ=π/2+η into Eq. (16)
$\boldsymbol{\tau}_{J\_2c}$	calculated unit tangential vector of c at J by Eq. (5)
$\boldsymbol{\tau}_{L1\_2}$	unit direction vector of L_1 in the second coordinate system
$\boldsymbol{\tau}_{L2\_2}$	unit direction vector of L_2 in the second coordinate system
φ	angle between the projection of FO_2 on the plane X_2Y_2 and X_2-axis
ϕ	angle between the projection of EO_2 on the plane X_2Y_2 and X_2-axis